electrochem

MDPI

Article

Irreversibility of Ag | AgCl Reference Electrodes

Koichi Jeremiah Aoki and Jingyuan Chen *

Electrochemistry Museum, Kofu 400-0015, Japan; d930099@yahoo.co.jp
* Correspondence: jingyuanchn46@yahoo.co.jp; Tel.: +81-9082625425

Abstract

An Ag | AgCl redox couple has been thought to work as a reversible reference electrode, although metal dissolution often occurs irreversibly. This report examines the kinetics by means of ac-impedance of AgCl films at the Ag electrode. A brief result is that the reaction rate for conventional voltammetric currents is totally irreversible, although it can be enhanced with the thickness of the AgCl film. According to the frequency-dependence of the imaginary admittance, the double layer capacitance is determined only by the geometrical area of the Ag-electrode to exhibit 140 μF cm^{-2}. This value is caused by the delocalized charge of AgCl dipoles rather than by water dipoles. The charge transfer rate of $AgCl + e^- \leftrightarrow Ag + Cl^-$ was evaluated from the variation in the real admittance with the frequency to yield the charge transfer rate constant on the order of 10^{-9} cm s^{-1}. The rate constants increased with the surface density (Γ) of the deposited AgCl in proportion to $\Gamma^{0.3}$. The fractional power of the increase indicates that the reaction should occur not only at the geometrical area of the Ag-electrode but also at fluctuated Ag-particles in electric connection with the Ag-electrode, caused by percolation. The reversibility of Ag | AgCl can be realized at current densities smaller than 0.1 μA mm^{-2}, exemplified by 10 nA at a 0.3 mm disk. Then, Ag | AgCl can be used as a counter electrode in ultramicroelectrode techniques in a two-electrode system.

Keywords: silver chloride; charge transfer rate constant; double-layer capacitance; electric percolation; reference electrode

1. Introduction

A film of silver chloride on a silver metal immersed in a given concentration of Cl^-, denoted by Ag | AgCl, has been extensively used as a reference electrode because it shows not only (A) high reproducibility and repeatability but also (B) high reversibility [1,2]. The (A) can be successfully accomplished by improving the construction of cell geometry and fabrication techniques with the aim of miniaturization [3–8]. In contrast, the (B) belongs to a thermodynamic or a kinetic subject, pertaining to the chemical reaction rate of $AgCl + e^- \leftrightarrow Ag^0 + Cl^-$. A delay of the reaction can be neglected when voltammetric currents through a voltage follower are extremely small in a three-electrode cell. However, the miniaturization by incorporating a counter electrode into a reference one [4,6,9–11] makes currents of nA order flow through the reference electrode. Then, a question arises on how much intensity of the current alters the potential of the reference electrode.

The homogeneously bimolecular reaction rate of Ag^0 with Cl^- has been reported to be 20 M^{-1} s^{-1} (M = mol dm^{-3}) [12], which corresponds to a reaction period of 0.05 s for $[Cl^-]$ = 1 M. Application of this time scale to electrochemical measurements ought to cause a delay of potential responses as slow as 0.05 s or 3 Hz. The slow rate is due to the

Academic Editor: Michael Lyons

Received: 4 June 2026
Revised: 11 July 2026
Accepted: 20 July 2026
Published: 22 July 2026

bond-breaking and the formation of Ag and Cl after the charge transfer. This is in contrast to fast charge transfer rates of outer-sphere metal complexes without rearrangement of molecular structure [13], exemplified by ferrocenyl complexes. Heterogeneous reactions are generally slower than homogeneous ones because reactants in different phases can meet only at an interface, while homogeneous reactants collide more freely and frequently [14]. As a result, a heterogeneous reaction at Ag | AgCl should exhibit a further delay over 0.05 s. The electrochemically determined heterogeneous charge transfer rates have been reported in the form of exchange current densities, j_0, which depend on measurement techniques and their analysis, as presented in Table 1. They are so widely scattered that it is difficult to estimate even the order of the reversibility. One reason for the scattering is alteration of the electrode surface during the reaction. It is desirable to evaluate explicitly the heterogeneous rates of AgCl without altering the thickness of AgCl films.

Table 1. Reported exchange current density of Ag | AgCl.

j_0/mA cm^{-2}	Techniques	Rate Determining Step	Ref.
0.13	quasi-steady-state *I*–V curves	mixed activation–ohmic step	[15]
100	chronopotentiometry	surface diffusion kinetics	[16]
30–110	ac-impedance	change in [Cl$^-$] by resistance of AgCl	[17]
4×10^{-5}–10^{-4}	Tafel slopes	porosity of AgCl	[18]

Here, we evaluate the charge transfer rates of Ag | AgCl electrodes to predict the stability of potentials at reference electrodes in the context of the thickness of the AgCl films. Our technique of the evaluation is ac-impedance, coupled with the concept of the constant phase element [19–23]. Since the redox current at Ag | AgCl electrodes has been enhanced with the thickness of the AgCl film [15], the rate per geometrical electrode area would be increased with the thickness. In order to grasp the reversibility, it is necessary to determine a quantitative relationship between the apparent heterogeneous reaction rate and the film thickness.

2. Materials and Methods

Three kinds of solutions were prepared: 0.2 M citric acid (M = mol dm^{-3}, pH 2.9) + 0.3 M NaCl, 0.05 M pH-buffered solution, (pH 7.0) + 0.45 M NaCl, and 0.2 M $NaHCO_3$ (pH 8.4) + 0.3 M NaCl. A silver wire 0.5 mm in diameter, the surface of which was polished, was inserted into a solution 5 mm in length by means of a z-stage. It was used as a working electrode. A reference and a counter electrode were an Ag | AgCl in the solution of [Cl$^-$] = 0.3 M and a platinum coil, respectively.

A constant current, ranging from 1 μA to 2 mA, was applied to the Ag wire to form an AgCl film at a given deposition time, t_{dp}, (from 4 s to 20 s). The product of the current and the time provides the theoretical thickness of AgCl through $jW_M t_{dp}/Fd$ [17], where j is the current density, W_M is the molar weight, F is the Faraday constant, and d is the density of AgCl. A typical thickness is 0.27 nm for j = 0.1 mA cm^{-2} at t_{dp} = 1 s. The thickness here is different from an averaged geometrical thickness, partly because our AgCl surfaces were rough by an optical microscopic view and partly because the density varies from point to point. A Γ-value may well be representative of a thickness. We express the surface density of AgCl as:

$$\Gamma = jt_{dp}/F \quad (1)$$

Ac-impedance was measured at the open circuit potential under the conditions of the ac-amplitude, 10 mV, and of the frequency domain from 1 Hz to 4 kHz. After the

ac-impedance measurement, cyclic voltammetry was made at several scan rates in order to confirm the amount of the deposited AgCl.

3. Results and Discussion

Figure 1A shows a cyclic voltammogram in the NaCl solution at pH 7. This voltammogram was almost the same as those for the other pH solutions except for peak potentials, for example, the anodic peak potential at 0.54 V for pH 7 being shifted by 0.05 V/pH. The sudden rise in the anodic current at E = 0 V is a well-known feature of dissolution [24] of metal, generating AgCl on the surface. The anodic current decreased after exhibiting a peak, probably because of a loss of diffusional supply of Cl^-. In contrast, the cathodic wave starting at 0 V is caused by the reduction of AgCl. The deposited AgCl is consumed at −0.9 V to generate Ag^0, and then the cathodic current drops after passing through the peak. Values of the peak potentials included too large IR-drop owing to the solution resistance (30 Ω) to discuss the peak-potential shifts in Figure 1A with variations in Cl^- and scan rates. Figure 1B shows voltammograms in the narrow potential domain at three scan rates. The narrow potential domain was selected so that the kinetic effect may be exhibited specifically without being disturbed by mass transport-controlled currents. The anodic currents and the cathodic ones were almost independent of the scan rates. Therefore, the currents should be controlled by chemical reaction rates rather than mass transport. The forward cathodic current near 0 V (Figure 1B(d)) is connected smoothly with the anodic one without any clear overpotential, suggesting an apparently reversible reaction. Since the cathodic waves at the forward scan intersected with those at the backward one, the oxidation of Ag^0 should occur faster than the reduction of AgCl. As a result, kinetics ought to be detected even at scan rates as slowly as 0.03 V s^{-1} (=v_0). This scan rate corresponds to the period, RT/Fv_0, which provides the rate $\delta/(RT/Fv_0)$ passing through a distance δ. A typical value of the rate calculated from $\delta/(RT/Fv_0)$ is 10^{-7} cm s^{-1} for δ = 1 nm of a AgCl film. It belongs to one of the slowest charge transfer reaction couples.

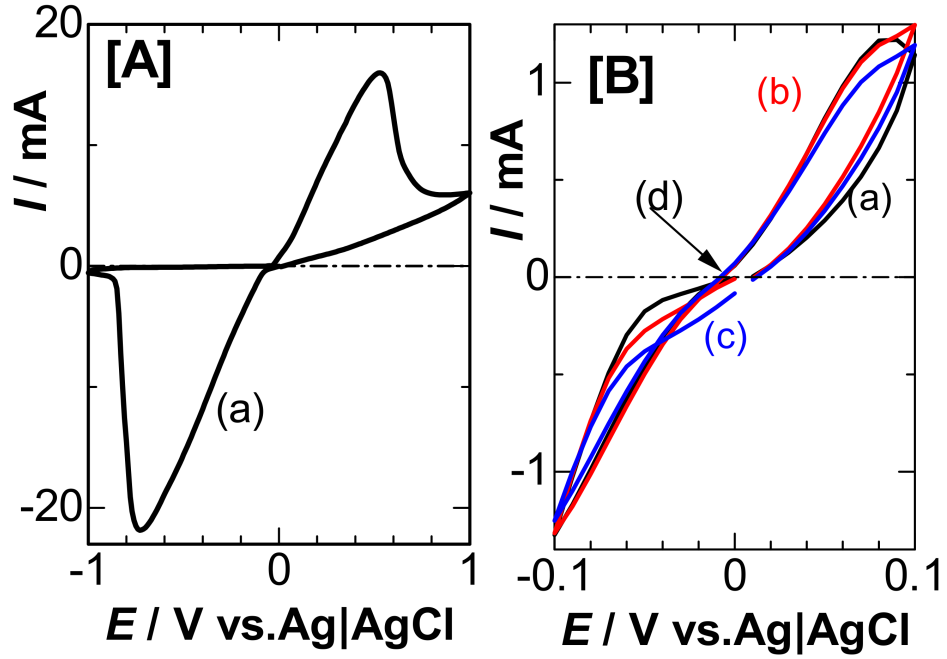

Figure 1. Cyclic voltammograms at the Ag working electrode in NaCl solution 0.45 M with pH 7 for v = (a) 0.03, (b) 0.1 and (c) 0.2 V s^{-1} in the (**A**) wide and (**B**) narrow domain. (**B**) (d) is the directing arrow near 0 V.

It is difficult to determine kinetic parameters quantitatively from such large voltammetric currents as for dissolution of metals. The difficulty can be covercome with a usage of ac-impedance when it is observed at an open-circuit dc-potential (OCP), E_{dc}. We made it for the frequency (f) domain from 1 Hz to 4 kHz. Figure 2A shows the Nyquist plots at the Ag-electrode coated with various amounts of AgCl, Γ, obtained for an OCP, where Z_1 and Z_2 are the real and the imaginary impedance, respectively. The value of Z_1 at which $-Z_2$ was extrapolated to zero was ca. 30 Ω, independent of Γ. This independence implies that the resistance should be due to the solution resistance, R_s rather than film resistance [15,17]. Plot (a), measured without deliberately forming any AgCl film takes a line with a slope of 7, which is the inverse of the exponent of the constant phase element. The linearity with the large slope represents the constant phase element [19–23] or the power–law of the frequency [25,26], which can discriminate against a vertical line for an ideal capacitance. The complex admittance of the double layer capacitance (DLC) with the power–law has been expressed by [26]

$$Y_{DLC} = (\lambda + i)\omega C_{1Hz} f^{-\lambda} \quad (2)$$

for $\omega = 2\pi f$, where λ is a positive constant near 0.1, i is the imaginary unit, and C_{1Hz} is the capacitance at f = 1 Hz. Figure 2B shows logarithmic plots of Y_1 and Y_2 against f for several values of Γ, where R_s was subtracted from Z_1 through $Y = 1/(Z - R_s)$, and Y_1 and Y_2 are the real and the imaginary parts of Y, respectively. Values of $\log(Y_2)$ were approximately linear with $\log f$, almost independent of Γ, as supported by the power law ($Y_2 = 2\pi C_{1Hz} f^{1-\lambda}$) in Equation (2). The value of λ was close to 0.1, as is similar to platinum electrodes in polarizable electrolytes [27]. The intercept of plot (a) without deliberately generated AgCl gave a value of C_{1Hz} of (150 ± 10) μF cm^{-2}, which is four times larger than that of a platinum electrode. The four times increase is ascribed partially to the dipole moment of AgCl (6.0 Debye [28]) which is 3.2 times larger than that of water and partially to an increase in surface roughness by metal dissolution [18].

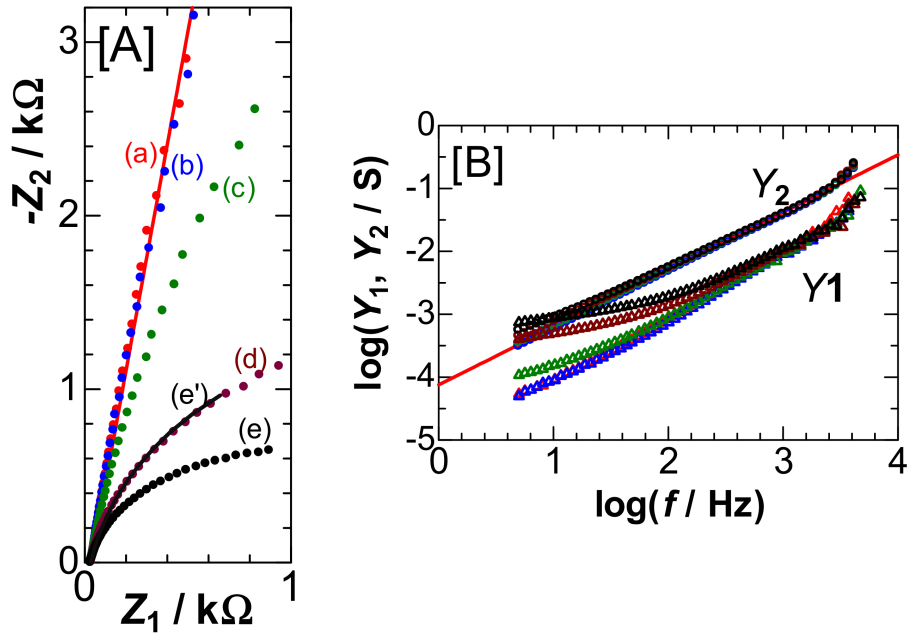

Figure 2. Nyquist plots (**A**) and the frequency dependence of Y (**B**) at the Ag wire electrode for Γ = (a) 0, (b) 5.2 × 10^{-10}, (c) 1.6 × 10^{-9}, (d) 5.2 × 10^{-9}, (e) 1.7 × 10^{-8} mol cm^{-2}. Open-circuit potentials were (a) −0.065, (b) 0.025 and (c)–(e) 0.004 V in the solution of pH 7. Line (e′) was computed from Equation (6). The colors of (**B**) are the same as (**A**) at the same Γ.

With an increase in Γ, values of $-Z_2$ decreased (Figure 2A) or those of Y_1 at low frequencies increased (Figure 2B) from the lines, because the charge transfer resistance, R_{ct}, of $Ag + Cl^- \leftrightarrow AgCl + e^-$ becomes conspicuous. Then the equivalent circuit may be approximated as the parallel combination of R_{ct} and Y_{DLC} [29]. The total admittance is expressed by:

$$Y \equiv Y_1 + iY_2 = \{\lambda\omega C_{1Hz} f^{-\lambda} + 1/R_{ct}\} + i\omega C_{1Hz} f^{-\lambda} \quad (3)$$

which yields $Z = R_{ct}(\lambda x + 1 - ix)/\{(\lambda x + 1)^2 + x^2\}$ for $x = 2\pi C_{1Hz} f^{1-\lambda} R_{ct}$. Eliminating x provides

$$(Z_1 - R_{ct}/2)^2 + (Z_2 - \lambda R_{ct}/2)^2 = (R_{ct}/2)^2 (1 + \lambda^2) \quad (4)$$

A variation of $-Z_2$ with Z_1 takes obviously a circle in the Nyquist plot, passing through the origin, as shown in Figure 3 [30,31]. Since values of $-Z_2$ are positive, an observed circle should be limited to the domain of the first quadrant. From the comparison of the variations in Figure 1A with those in Figure 3, values of R_{ct} decrease with an increase in Γ for a positive value of λ.

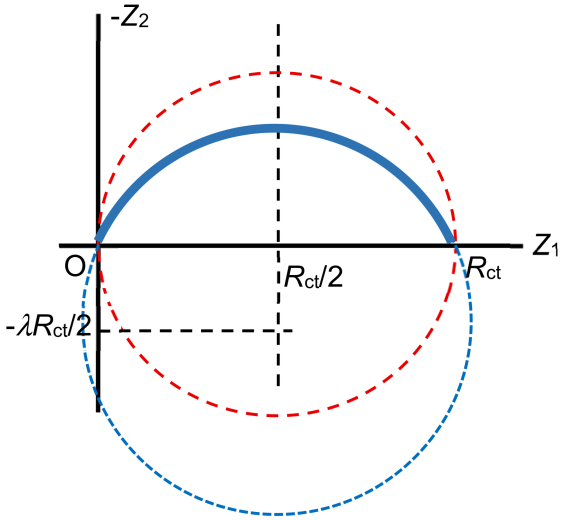

Figure 3. Illustration of a shift in semicircles expressed by Equation (3) for $\lambda = 0$ (red dashed) and 0.5 (blue solid).

Our aim is to evaluate R_{ct} and C_{1Hz} as a function of Γ by use of Equation (3) or (4). Although Equation (4) is mathematically equivalent to Equation (3), it does not include frequency-dependence explicitly. The frequency-dependence in Equation (3) can be examined through linearity of $\log Y_2$ with $\log f$, whereas Equation (4) is limited to curve-fitting without examination of the dependence [32,33]. We apply the admittance to Equation (3), paying attention to the frequency-dependence. Values of λ determined from the plot of $\log Y_2$ vs. $\log f$ were almost constant (0.09) for $\log \Gamma < -6.5$ in Figure 4, where the lowest Γ corresponds to a monomolecular layer of the AgCl film. The constant means that Y_2 should be controlled by the conventional frequency dispersion (Equation (2)). The intercept of the $\log Y_2$ vs. $\log f$ (Figure 2B) provides C_{1Hz}, according to Equation (3). The variation in the thus evaluated C_{1Hz} with $\log(\Gamma)$ is shown in Figure 4. Values of C_{1Hz} range from 140 to 160 $\mu F\ cm^{-2}$, being almost independent of Γ. Therefore, the DLC should be provided only with the geometrical surface area of the Ag electrode. The gradual increase in C_{1Hz} with $\log\Gamma$ may be ascribed to enhancement of the surface roughness caused by the iterative surface ac-modulation in the series of experimental runs.

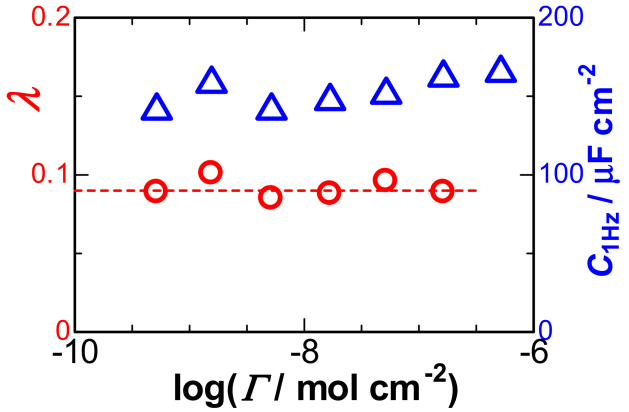

Figure 4. Variations of λ (circles) and $C_{1\mathrm{Hz}}$ (triangles) with $\log(\Gamma)$, obtained from Figure 2B.

The real part in Equation (3) indicates that $\log Y_1$ is not linear with $\log f$ owing to $1/R_{\mathrm{ct}}$. The equation of $\log Y_1$ can be approximated for high frequency and large values of R_{ct} as

$$\log Y_1 \approx (1-\lambda)\log f + \log(2\pi C_{1\mathrm{Hz}}) + 1/(R_{\mathrm{ct}}2\pi\lambda C_{1\mathrm{Hz}} f^{1-\lambda}) \quad (5)$$

It suggests a linear plot of $\log Y_1$ against $\log f$ at high frequency with a slope of $1-\lambda$ and an intercept of $\log(2\pi C_{1\mathrm{Hz}}) + 1/(R_{\mathrm{ct}}2\pi\lambda C_{1\mathrm{Hz}})$ for a known value of λ. The intercept gives values of R_{ct} from the known values of λ and $C_{1\mathrm{Hz}}$. Since values of R_{ct} are often proportional to experimentally used electrode areas, A, they are not universally physicochemical parameters. A universal, kinetic parameter is the exchange current density through $j_0 = RT/FR_{\mathrm{ct}}A$. Figure 5 shows the plot thus determined variation of j_0 against Γ, which can be represented by an empirical relation,

$$j_0/\mathrm{A\ cm^{-2}} = 1.86 \times 10^{-4}\,(\Gamma/\mathrm{mol\ cm^{-2}})^{0.3} \quad (6)$$

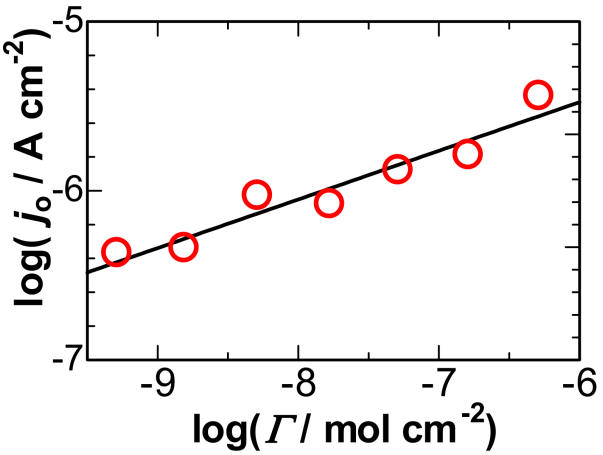

Figure 5. Logarithmic variation of j_0 with Γ, obtained from Equation (5).

The fractional power of Γ in Equation (6) implies that the reaction could occur mainly at a fluctuated surface of Ag particles electrically connected to the Ag electrode rather than the plateau of the Ag electrode, as illustrated in Figure 6. For example, Ag particles described by open circles in Figure 6 cannot work as an electrode because of a loss of electric connection to the Ag electrode blocked by the insulator of AgCl (filled squares). On the other hand, the Ag particles with the filled circles have electric connection to the electrode. The latter can function as a surface for the electrode reaction.

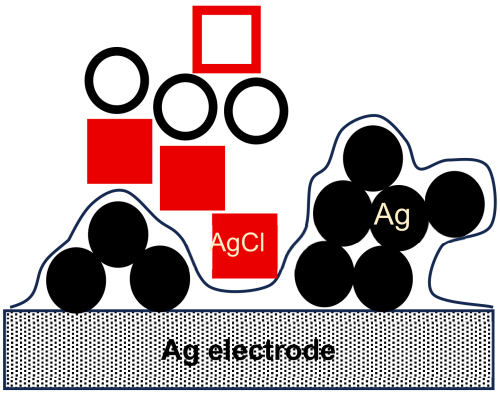

Figure 6. Illustration of an AgCl film mixed with AgCl particles (squares) and Ag particles (circles), where the filled circles are electrically percolated to the electrode and open ones are not.

The area of the boundary between the electrically connected Ag particles and the solution is increased with an increase in the film thickness, exhibiting fluctuated rough surfaces [34]. The ratio of the boundary area to the geometrical Ag area is proportional to the fractional power (0.3) of the thickness. Electrode reactions associated with electrical connection or disconnection have been found to generate fluctuated surfaces, as observed in iterative redox reactions of polyaniline films [25,26,35]. Although this larger area should generate a capacitance, C_{connect}, larger than $C_{1\text{Hz}}$ (140 $\pm$ 10 μF cm^{-2}), C_{connect} cannot be observed because the inverse of the detected capacitance is $1/C_{\text{connect}} + 1/C_{1\text{Hz}}$.

The smallest value of Γ (=5.2 $\times$ 10^{-10} mol cm^{-2}) may correspond to a monolayer adsorption of AgCl. The smallest j_0 $-$ value ($j_{0\text{sm}}$ = 4.3 $\times$ 10^{-7} A cm^{-2}) for this Γ can be regarded as a physicochemically significant quantity for discussing the standard charge transfer rate constant k^0 through $j_0 = Fk^0c = Fk^0\Gamma/\delta$, where c is the concentration of a redox species, and δ is a distance between neighboring adsorbed redox species, 0.56 nm for a crystalline AgCl. It can be also expressed by Equation (6). Extracting k^0 using the density $d = \Gamma W_{\text{M}}/\delta$ yields

$$k^0 = (1.86 \times 10^{-4}\ \text{A cm}^{-2}) W_{\text{M}} \Gamma^{0.3}/Fd = 2.8 \times 10^{-7} \Gamma^{0.3}\ \text{cm s}^{-1} \quad (7)$$

for d = 1 g cm^{-3} in the right term. When AgCl films are 10 times, 10^2 times and 10^4 times larger than that of monolayer, the values of k^0 are 1 $\times$ 10^{-9}, 2 $\times$ 10^{-9} and 7 $\times$ 10^{-9} cm s^{-1}, respectively. These values belong to the totally irreversible domain, although the power (0.3) of Γ in Equation (7) can slightly enhance the reversibility with an increase in the thickness. These determined values are much smaller than those (Table 1) reported so far. A main reason for the smallness is that the fractal area of the Ag particles is much larger than the geometrical area of the electrode.

An Ag | AgCl reference electrode has been used for a miniaturized two-electrode cell [4,6,9–11], where it is assumed to cause reversible reactions. This assumption is based on the kinetic equation in which an overpotential ought to be depressed with a decrease in the current density. In order to keep consistency between the irreversibility and the small current density, we discuss here a relationship between current values at microelectrodes and the allowed overpotentials. When a current of 1 nA flows in an Ag | AgCl electrode, values of R_{ct} ranging from 0.1 MΩ to 1 MΩ provide the interfacial voltages from 1 mV to 10 mV, which may be neglected in practical voltammetry. Thus, Ag | AgCl reference electrodes would be used as counter electrodes for a two-electrode cell configuration, as has been carried out in the miniaturization of reference electrodes [36] without counter electrodes in a two-electrode cell [4,6]. It is worthwhile to examine this prediction quantitatively. It is assumed that the current I flows through both a working and a reference electrode in

a two-electrode cell. The voltage at R_{ct} is given by $\Delta V = IR_{ct} = I(RT/FAj_0)$ with the help of $j_0 = RT/FR_{ct}A$, where A is the area of the reference electrode. When Equation (6) is inserted into the above j_0, the condition of keeping $\Delta V < 1$ mV is $(RT/F)(I/A)(10^4/1.86\ \Gamma^{0.3}) < 1$ mV or

$$I/A\Gamma^{0.3} < 0.72 \times 10^{-5} \quad (8)$$

at 25 °C at the units of ampere for I, cm^2 for A and mol cm^{-2} for Γ. Examples of the maximum area of Ag | AgCl for some combinations are shown in Table 2. They are just tentative estimations, but they may be complicated by competition between the kinetics of AgCl and mass transport rate/mode of redox species. Kinetic values determined by ac-impedance are generally influenced by uncompensated resistance, double layer charging currents, ambiguity in the relationship between electric elements and electrochemical components, and inadequate equivalent circuits. Consideration of the first two effects leads to enhanced rate constants. The third effect includes an effective area of an electrode, which corresponds to the fractal surface area.

Table 2. Maximum areas (mm^2) for satisfying $\Delta V < 1$ mV for some values of I and Γ.

Γ/mol cm^{-2}	I = 1 nA	I = 10 nA
10^{-8}	3.5	35
10^{-7}	0.017	0.17
10^{-6}	0.01	0.09

4. Conclusions

The electrochemical reaction between Ag and AgCl has the standard rate constant on the order of 10^{-9} cm s^{-1}, which belongs to the totally irreversible domain. However, it has been extensively used as a reversible reference electrode. The contradiction results from the magnitude of the currents in a two-electrode cell; normal voltammetric currents of μA order in magnitude yield a 1 V voltage drop at the interface for R_{ct} = 1 MΩ, whereas currents of 1 nA order yield only a 1 mV voltage drop across the interface. Therefore, microelectrode voltammetry can be carried out in a two-electrode cell.

The plots of logY_2 vs. log f, which can represent the properties of the DLC, took a line independent of values of Γ. Thus, the DLC should be determined only by the area of the Ag-electrode. The value of the DLC is 140 μF cm^{-2}, which is caused by the delocalized charge of AgCl dipoles rather than by water dipoles. In contrast, R_{ct} evaluated from the logarithmic plots of Y_1 vs. f varies with the film thickness, although it is a property of an electrode | solution interface. This interface is not for the DLC at the planar Ag-lectrode | solution but is for the charge transfer at the fluctuated surface of Ag-particles electrically percolated to the electrode.

Author Contributions: Conceptualization, K.J.A.; methodology, K.J.A. and J.C.; investigation, K.J.A. and J.C.; writing—original draft preparation, K.J.A.; writing—review and editing, K.J.A. and J.C.; supervision, K.J.A.; project administration, J.C.; funding acquisition, K.J.A. and J.C. All authors have read and agreed to the published version of the manuscript.

Funding: This research received no external funding.

Institutional Review Board Statement: Not applicable.

Informed Consent Statement: Not applicable.

Data Availability Statement: The raw data supporting the conclusions of this article will be made available by the authors on request. Ask K.J.A. at d930099@yahoo.co.jp.

Conflicts of Interest: The authors declare no conflicts of interest.

References

1. Ives, D.J.G.; Janz, G.J. *Reference Electrodes: Theory and Practice*; Academic Press Inc.: New York, NY, USA, 1961.
2. Maksimov, I.; Asakai, T.; Ohata, M. On the optimal use of silver–silver chloride reference electrodes. *Accred. Qual. Assur.* **2023**, *28*, 65–68. [CrossRef]
3. Dawkins, R.C.; Wen, D.; Hart, J.N.; Vepsalainen, M. A screen-printed Ag/AgCl reference electrode with long–term stability for electroanalytical applications. *Electrochim. Acta* **2021**, *393*, 139043. [CrossRef]
4. Lee, Y.-G.; Han, J.; Kwon, S.; Kang, S.; Jang, A. Development of a rotary disc voltammetric sensor system for semi-continuous and on-site measurements of Pb(II). *Chemosphere* **2016**, *143*, 78–84. [CrossRef] [PubMed]
5. Shinwari, M.W.; Zhitomirsky, D.; Deen, I.A.; Selvaganapathy, P.R.; Deen, M.J.; Landheer, D. Microfabricated Reference Electrodes and their Biosensing Applications. *Sensors* **2010**, *10*, 1679–1715. [CrossRef] [PubMed]
6. Lee, Y.-G.; Jang, A.J. Effect of the working and counter/quasi-reference electrode relative area ratio of silver sensor electrodes on voltammetric detection of Pb(II). *Ind. Eng. Chem.* **2020**, *81*, 67–70. [CrossRef]
7. Zhao, Z.; Tu, H.; Kim, E.G.R.; Sloane, B.F.; Xu, Y. A flexible Ag/AgCl micro reference electrode based on a parylene tube structure. *Sens. Actuators B* **2017**, *247*, 92–97. [CrossRef]
8. Brewer, P.J.; Brown, R.J.C. Effect of Structural Design of Silver/Silver Chloride Electrodes on Stability and Response Time and the Implications for Improved Accuracy in pH Measurement. *Sensors* **2009**, *9*, 118–130. [CrossRef] [PubMed]
9. Brewer, M.G.; Baldi, A.; Merlos, A.; Sanchez, C.F. Array of individually addressable two-electrode electrochemical cells sharing a single counter/reference electrode for multiplexed enzyme activity measurements. *Bios. Bioelect.* **2022**, *201*, 113952.
10. Xu, Q.; Xi, Y.; Wang, L.; Xu, M.; Ruan, T.; Du, Z.; Jiang, C.; Cao, J.; Zhu, X.; Wang, X.; et al. In situ self-referenced intracellular two-electrode system for enhanced accuracy in single-cell analysis. *Bios. Bioelect.* **2024**, *253*, 116173. [CrossRef]
11. Wang, N.; Wang, D.; Pan, R.; Wang, D.; Jiang, D.; Chen, H.-Y. Self-Referenced Nanopipette for Electrochemical Analysis of Hydrogen Peroxide in the Nucleus of a Single Living Cell. *Anal. Chem.* **2021**, *31*, 10744–10749. [CrossRef]
12. Miah, M.R.; Sen, D.; Rahman, M.A.; Siddiquey, I.A.; Alam, M.M. Conductometric Studies of Kinetics of Ionic Reaction between Ag and Cl in Aqueous Solution. *Int. J. Sci. Tec. Res.* **2017**, *6*, 52–56.
13. Neha; Kant, R. Theory for Outer Sphere Electron Transfer Coupled with Ion Transfer Kinetics on Atomically Stepped Metal. *J. Phys. Chem. C* **2024**, *128*, 12399–12413. [CrossRef]
14. Poovan, F.; Chandrashekhar, V.G.; Natte, K.; Jagadeesh, R.V. Synergy between homogeneous and heterogeneous catalysis. *Catal. Sci. Technol.* **2022**, *12*, 6623–6649. [CrossRef]
15. Ha, H.; Payer, J. The effect of silver chloride formation on the kinetics of silver dissolution in chloride solution. *Electrochim. Acta* **2011**, *56*, 2781–2791. [CrossRef] [PubMed]
16. Despic, A.R.; Bockris, J.O.M. Kinetics of the deposition and dissolution of silver. *J. Chem. Phys.* **1960**, *32*, 389. [CrossRef]
17. Tjon, K.C.E.; Yuan, J. Impedance characterization of silver/silver chloride micro-electrodes for bio-sensing applications. *Electrochim. Acta* **2019**, *320*, 134638. [CrossRef]
18. Lu, X.; Hu, J.; Feng, X.; Zhou, Q.; Qu, Z.; Zhang, J.; Zhu, R.; Zhang, H.; Chen, S. Long-Lifetime Ag/AgCl Electrodes Prepared by Pulse Current Electrodeposition for Chloride Monitoring in the Concrete Environment. *Sensors* **2025**, *25*, 5032. [CrossRef] [PubMed]
19. Lasia, A. Electrochemical Impedance Spectroscopy and its Applications. In *Modern Aspects of Electrochemistry*; White, R.E., Conway, B.E., Bockris, J.O'M., Eds.; Kluwer Academic/Plenum Publishers: New York, NY, USA, 1999; Volume 32, p. 143.
20. Brug, G.J.; Van Den Eeden, A.L.G.; Sluyters-Rehbach, M.; Sluyters, J.H. The analysis of electrode impedances complicated by the presence of a constant phase element. *J. Electroanal. Chem.* **1984**, *176*, 275–295. [CrossRef]
21. Zoltowski, P. On the electrical capacitance of interfaces exhibiting constant phase element behaviour. *J. Electroanal. Chem.* **1998**, *443*, 149–154. [CrossRef]
22. Nyikos, L.; Pajkossy, T. Fractal dimension and fractional power frequency-dependent impedance of blocking electrodes. *Electrochim. Acta* **1985**, *30*, 1533–1540. [CrossRef]
23. Schalenbach, M.; Durmus, Y.E.; Robinson, S.A.; Tempel, H.; Kungl, H.; Eichel, R.A. Physicochemical Mechanisms of the Double-Layer Capacitance Dispersion and Dynamics: An Impedance Analysis. *J. Phys. Chem. C* **2021**, *125*, 5870–5879. [CrossRef]
24. Low, C.T.J.; de Leon, C.P.; Walsh, F.C. Copper deposition and dissolution in mixed chloride–sulphate acidic electrolytes: Cyclic voltammetry at static disc electrode. *Trans. IMF* **2015**, *93*, 74–81. [CrossRef]
25. Aoki, K.; Cao, J.; Hoshino, Y. Logarithmic Relaxation of Electrochemical Insulating-to-Conducting Conversion at Polyaniline Films: Interpretation by Electric Percolation. *Electrochim. Acta* **1994**, *39*, 2291–2297. [CrossRef]
26. Han, T.; Song, T.; Gan, J.; Han, D.; Niu, L. Frequency Dependence of Effective Capacitance *Cec* for Polyaniline Membrane-Based pH Sensor and its Extension to the Gouy–Chapman–Stern Model. *Electrochem* **2026**, *7*, 10. [CrossRef]
27. Hou, Y.; Aoki, K.J.; Chen, J.; Nishiumi, T. Invariance of double layer capacitance to polarized potential in halide solutions. *Univ. J. Chem.* **2013**, *1*, 162–169. [CrossRef]
28. Nair, R.K.P. Electric dipole moment of the diatomic AgCl molecule. *J. Phys. B* **1985**, *17*, 735.

29. Das, S.; Banerjee, A.; Nandi, U.; Ghosh, A. Critical review on the analysis of electrochemical impedance spectroscopy data. *J. Appl. Phys.* **2025**, *138*, 125002. [CrossRef]
30. Abouzari, M.R.S.; Berkemeier, F.; Schmitz, G.; Wilmer, D. On the physical interpretation of constant phase elements. *Solid State Ion.* **2009**, *180*, 922–927. [CrossRef]
31. Mulder, W.H.; Sluyters, J.H. An explanation of depressed semi-circular arcs in impedance plots for irreversible electrode reactions. *Electrochim. Acta* **1988**, *33*, 303–310. [CrossRef]
32. Huang, J.; Li, Z.; Liaw, B.Y.; Zhang, J. Graphical analysis of electrochemical impedance spectroscopy data in Bode and Nyquist representations. *J. Power Sources* **2016**, *309*, 82–98. [CrossRef]
33. Lazanas, A.C.; Prodromidis, M.I. Electrochemical Impedance Spectroscopy—A Tutorial. *ACS Meas. Sci.* **2023**, *3*, 162–193. [CrossRef]
34. Stauffer, D. *Introduction to Percolation Theory*; Taylor and Francis: London, UK, 1985.
35. Aoki, K.; Aramoto, T.; Hoshino, Y. Photographic measurements of propagation speeds of the conducting zone in polyaniline films during electrochemical switching. *J. Electroanal. Chem.* **1992**, *340*, 127–135. [CrossRef]
36. Kahlert, H. Chapter 11, Micro-reference Electrodes. In *Handbook of Reference Electrodes*; Inzelt, G., Ed.; Springer: Berlin/Heidelberg, Germany, 2013.